Loop engineering of a thermostable GH10 xylanase to improve low-temperature catalytic performance for better synergistic biomass-degrading abilities

Jun Wang (wangjun@just.edu.cn)
Jiangsu University of Science and Technology
Shuai You
Jiangsu University of Science and Technology: Jiangsu University
Ziqian Zha
school of biotechnology, jiangsu University of Science and Technology
Jing Li
department of nephrology, affiliated hospital of jiangsu university
Wenxin Zhang
school of biotechnology, jiangsu university of science and technology
Zhiyuan Bai
school of biotechnology, jiangsu university of science and technology
Yanghao Hu
school of biotechnology, jiangsu university of science and technology
Xue Wang
school of biotechnology, jiangsu university of science and technology
Yiwen Chen
school of biotechnology, jiangsu university of science and technology
Zhongli Chen
Xinyuan cocoon silk group co., ltd.
Huiying Luo (luohuiying@caas.cn)
Chinese Academy of Agricultural Sciences Institute of Animal Science

Research

Keywords: GH10 xylanase, Low-temperature catalytic performance, Thermostability, Synergism, Biomass degradation

Posted Date: May 6th, 2021

DOI: https://doi.org/10.21203/rs.3.rs-466274/v1

Abstract

Background

Xylanase can efficiently hydrolysis of hemicellulose, a barrier to the efficient saccharification of lignocellulose, into xylooligosaccharides and is widely used in the fields of feed, food and biomass utilization. High-temperature xylanase usually has low catalytic activity below 40°C, which limits its applications. Therefore, improving the properties of xylanases to enable synergistic degradation of lignocellulosic biomass with cellulase is of considerable significance in the field of bioconversion of lignocellulosic biomass.

Results

In this study, a structure-based rational design strategy was applied to enhance the low-temperature catalytic performance of XYL10C_ΔN (WT). Screening and comparison were performed amoung the WT and mutants. In comparison with WT, MF53/53SL + N207G exhibited higher specific activity (2.9-fold; 2090 *vs.* 710 U/mg) and catalytic efficiency (2.8-fold; 1530 *vs.* 550 mL/s·mg) at 40°C, as well as higher thermostability (with T_m and T_{50} increased by 7.7°C and 3.5°C, respectively). Meanwhile, comparing with cellulase-only treatment, the combination of MF53/53SL + N207G and cellulase increased the reducing sugar by 1.6-, 1.2-, and 1.4-folds for degradating corn stalk, wheat bran, and corn cob, with the highest degree of synergy of 1.9, 1.2, and 1.6, respectively.

Conclusions

This study provided a successful strategy to improve the catalytic properties of enzymes and identified loop2 is a key functional area that affects the low-temperature catalytic efficiency of GH10 xylanase. Several xylanase candidates for applications in feed and bioenergy applications were obtained. Synergistic degradation experiments elucidated a possible mechanism of cellulase inhibition by xylan during the hydrolysis of different types of biomass.

Highlights

1. Discovered key amino acid sites that promote enzyme catalytic efficiency at 40 ℃.
2. Thermostable mutants with high catalytic efficiency at 40 °C were obtained.
3. The synergistic effect of xylanase and cellulase were significantly improved.
4. Three agricultural wastes were converted to reduce saccharide via enzymatic hydrolysis

Background

The increase in environmental pollution has correspondingly increased the demand for renewable and clean fuels to replace the traditional fossil fuels over the last few decades. A preferred alternative is the production of ethanol through fermentation of biological resources after enzymatic hydrolysis. Lignocellulosic biomass is considered as a vital asset for the production of renewable energy, because it is widely abundant, inexpensive, and environmentally friendly [1]. Lignocellulosic biomass has a rigid and complex structure, which is primarily composed of crystalline cellulose (38–50%), hemicellulose (23–32%), and lignin (15–25%), making it resistant against biological attacks [2]. Like cellulose, xylan is also one of the primary biofuel materials. Its products (xylose and xylo-oligosaccharides) from biomass degradation can be fermented by *Saccharomyces cerevisiae* and other genetically engineered microorganisms for the production of ethanol or other advanced biofuels [3]. The conversion of renewable lignocellulosic materials into biofuels through enzymatic decomposition is a sustainable and environmentally friendly alternative to natural fossil fuels. This process requires the cooperation of cellulolytic and xylanolytic enzymes, of which endo-cellulase and endo-xylanase are the main enzymes that hydrolyze the main chains of cellulose and xylan, respectively [4]. However, enzyme catalytic activity, thermal stability, the combination of different types of enzymes, and the pretreatment process of biomass are the key factors that affects the efficiency of biomass saccharification. Therefore, research efforts on the bioconversion of lignocellulosic biomass into biofuels are focused on the development of enzymes with outstanding properties and cost-effective optimization processes [5].

Xylan, one of the most abundant and important renewable bioresource, accounts for approximately 35% of the dry weight of plant cell walls and can be permanently attached to the surface of cellulose, which hinders the access of cellulase to cellulose during the enzymatic hydrolysis of biomass. Therefore, in conventional (or present) lignocellulosic biomass deconstruction systems, the addition of accessory enzymes such as xylanase is a feasible and effective alternative [6]. The steady increase in the requirement of xylanase is mainly due to its high demand in a variety of industries, such as animal feed, food processing, biofuels, pulp bleaching, and beer brewing. Xylanase hydrolyzes the 1,4-xylosidic bonds of hemicellulose to produce xylo-oligosaccharides, which can be used by different microorganisms, for the process of saccharification and the production of high-value metabolites [7]. Xylanases are distributed in 5, 7, 8, 10, 11, 30, and 43 families of glycoside hydrolases (GHs), based on sequence identity and three-dimensional structural homology. GH10 and GH11 xylanases have received the most attention in the literature thus far. GH11 xylanase exhibits a higher catalytic efficiency (~ 2–3 fold) than GH10. However, GH10 xylanase exhibits better thermostability than GH11, especially in animal body temperature (~ 40°C), which significantly limits its application in feed and other industrial fields [3]. Evidently, the combination of superior catalytic efficiency and high-temperature resistance can produce enzymes with excellent performance capabilities.

As of 2020, 53 crystal structures of GH10 xylanase and its mutants from several microorganisms have been successfully analyzed (http://www.cazy.org/GH10_structure.html). The catalytic domain of GH10 xylanase is a typical $(\beta/\alpha)_8$ TIM-barrel fold, in which the eight α-helices and eight parallel β-strands are connected by seven αβ or βα loops. The loops connecting the secondary structure are very flexible and

have different lengths, and the amino acid composition is weakly conserved. They are usually located on the surface of the protein and are critical to the catalytic activity and substrate specificity of the enzyme [8]. Many studies have been conducted to improve the catalytic efficiency of xylanases by the reconstruction of the loop region [9]. However, there are relatively few reports describing the influence of regional structure on the catalytic efficiency of xylanase. For example, the mutations developed by Pro-to-Leu and Val-to-Leu on the different loops of xylanase XT6 from *Geobacillus stearothermophilus* relating to substrate binding led to an increased catalytic efficiency by 5.7-and 6.5 fold, respectively [10]. By replacing the loop region, the catalytic efficiency and specific activity of xylanase XylE can be increased by three and 2.3 times respectively, and loop2, loop3, and loop6 were identified as the three key loop regions affecting the catalytic activity of the enzyme [11]. The results of these previous studies confirm that structural changes in the loops have a decisive effect on the catalytic efficiency of the enzyme. However, there are no studies on the improvement of the catalytic activity of thermotolerant xylanase at lower temperatures, such as 40°C. Rationally, the overall design of proteins must be based on a comprehensive and profound insight subject to enzyme conformation to enhance its thermostability and catalytic efficiency. Typically, low catalytic efficiency at industrial working temperatures impedes the effective utilization of an enzyme. Therefore, it is important to improve the catalytic efficiency of enzymes via protein engineering under specific conditions, such as directed evolution and rational or comprehensive design. However, the mechanism of catalytic activity based on structural conformation has not been completely analyzed, and there are no studies describing a standard and accurate method that enhances enzyme catalytic activity. In addition, most of the strategies used for improving enzyme molecules fail to consider the thermostability and catalytic efficiency of enzymes. Therefore, it is important to find a method that not only improves the catalytic efficiency but also maintains or enhances the thermostability of the enzyme.

XYL10C_ΔN is a xylanase with high specific activity, high catalysis, and high temperature resistance, which was revealed in our previous work. Its crystal structure was successfully analyzed (PDB: 5XZO/5XZU), and its catalytic activity at low temperatures (40°C) was less than 10% of the highest activity [12]. In this study, improved the activity of XYL10C_ΔN at a low temperature (40°C) and enhanced its thermostability by reshaping the structure of key loops based on rational design. Three single point mutations and their combined mutated enzymes exhibited substantial improvements in catalytic performance for specific substrates at 40°C and it either preserved or improved enzymatic thermostability relative to the mesophilic parent. Molecular dynamics (MD) simulations were used to analyze the structural basis of these changes, and the application potential of selected mutant enzymes in the degradation of agricultural lignocellulosic biomass waste was also evaluated.

Results And Discussion

Selection of the mutation site and site-directed mutagenesis

The loop regions of the TIM-barrel enzyme are considered to be invaluable for the interaction of the enzyme and the substrate [13]. Sequence evolution and three-dimensional conformation analysis

indicated that the Asn207 of XYL10C_ΔN (PDB entry: 5XZO/5XZU) [12] might be the key switch residues for controlling the movement of loop (α5-β6) and loop5 (Fig. 1). The catalytic performance of XYL10C_ΔN may be related to the conformational plasticity of this flexible structure. Therefore, based on the amino acid evolution information (Fig. S1), we mutated Asn207 to Gly, Glu, Ser, Asn, and Lys. Met53 and Phe54, located on loop2, form the only helical segment in this random coil. The conformation of the short helix may affect the expansion and contraction of loop2 in the catalytic channel, thereby affecting the catalytic activity of the enzyme. Sequence alignment analysis results show that although these two amino acids are not very conservative, there are a few noticeable changes. Therefore, based on the evolution of amino acids, we mutated M53/F54 to V53/S54, E53/S54, I53/S54, E53/R54, S53/Y54, G53/V54, M53/Y54, F53/A54, P53/A54, and A53/E54, and investigated the effects of all mutagenesis catalytic performances at low temperatures (40 °C).

Production and purification of recombinant XYL10C_ΔN and mutants

WT XYL10C_ΔN and its mutants were successfully expressed in *P. pastoris* GS115 and purified. Except for mutants MF53/54AA and MF53/54VV, which displayed no activity, enzyme activity was found in all the other mutants. After ion exchange purification according to “Materials and Methods,” MF53/54SL and N207G showed significant improvement in specific activities (1590 and 1000 U/mg vs. 710 U/mg) compared to that of the WT at 40 °C. Thus, single (MF53/54SL and N207G) and the combined (MF53/54SL+N207G) were expressed and characterized as described above.

SDS–PAGE analysis showed that the electrophoresis purity of all enzymes was over 95%, and the molecular masses were between 45 and 65 kDa, which is higher than the theoretical value (approximately 38.2 kDa). (Fig. S2). The difference between the apparent and theoretical molecular weights was because of the protein glycosylation modification [12].

Comparison of the pH properties andtemperature optima of XYL10C_ΔN and its mutants

Using beechwood xylan as the substrate, the effect of pH on the activity and stability of all enzymes was determined at 85 °C. As shown in Fig. 2A, the optimum pH for WT and its mutants was 4.0 or 4.5. This result was similar to that of GH10 xylanase obtained from most of the fungi, such as *Penicillium canescens* [14], *Trichoderma reesei* [15], and *Aspergillus nidulans* [16]. The relative activities of all the enzymes in the same pH environment were not significantly different. All enzymes approximately maintained more than 50% relative enzyme activity between pH 3 and 6. Notably, the pH range of the combination mutant MF53/54SL+N208G has increased, facilitating it to maintain more than 76% relative enzyme activity between pH 3.5, and 5.5, which is higher than that of the WT and the other two mutants. In terms of pH stability, all mutants were similar to the WT, and all the enzymes maintained > 50% of their maximal activity at pH ranging from 1 to 8 after incubation at 37 °C for 1 h (Fig. 2B). The excellent stability of all mutants under acidic conditions highlights their suitability for application in bioethanol, detergent, and feed additive industries [17].

The optimal temperature (T_{max}) of the enzymes was determined over a wide range of temperatures from 40 °C to 95 °C at their respective optimal pH with beechwood xylan as the substrate. Notably, as indicated in Fig. 2C, similar to 1VBU from *Thermotoga maritima* [8], the T_{max} of WT and its mutants, MF53/54SL and MF53/54SL+N207G, had an optimal temperature of 90 °C. The optimal temperature of the mutant N207G was 85 °C, which was 5 °C lower than that of the WT. *Aspergillus* [18] and *Penicillium* [3] are the two major sources of GH10 xylanases. As shown in table S1, the optimum temperature for xylanases derived from these two microorganisms is mostly between 50 and 75 °C, with the exception of *Thermotoga maritima*, having an optimum temperature of 90 °C.

Notably, a steady development of improved activity was observed in the mutants at lower temperatures than in the WT. For example, at 60 °C, all mutants showed 51% to 55% of the maximal activity, which was much higher than the result for the WT (~30% of the maximal activity). When the temperature decreased to 40 °C, three mutants, MF53/54SL, N207G, and MF53/54SL+N207G maintained 27%, 17%, and 26% of the activity, respectively, whereas the WT maintained only 9% of activity. The relative activity of the three mutants was 1.9-3.0 times higher than that of the WT. This indicates that mutations at these sites increase the catalytic activity of enzymes at low temperatures. As the environment of the animal digestive tract is at approximately 40 °C, the increase in relative enzyme activity of mutants at 40 °C is more conducive to the application of xylanase in feed supplements.

Kinetics and specific activity ofWT and its mutants at 40 °C

Research on GH10 xylanase has mainly focused on the heat-resistant mechanism and molecular improvement, and studies on the catalytic mechanism are relatively rare [19]. However, Xiong et al. mutated the N86 of the -2 substrate-binding region of GH10 xylanase to Gln, which enhanced the hydrogen bond interaction with the surrounding amino acids, enlarged the volume of the catalytic pocket, and eventually led to an increase in enzyme catalytic activity by a factor of 1.25 [20]. Through virtual mutation and MD simulation, Wu et al. introduced Glu and Asn into the catalytic center of xylanase, which enhanced the binding force of the substrate molecule and the catalytic channel, and finally increased the catalytic efficiency of the enzyme by 72% [21]. However, most research on the catalytic mechanism is concentrated on the catalytic center of the enzyme, and there have been no reports on the protein surface and loop area. In addition, previous studies have mainly focused on the changes in enzyme catalytic efficiency at the optimal temperature [22]. However, there are no studies on the improvement of catalytic activity at a specific application temperature. Xylanase for feed requires excellent thermal stability to ensure that it does not get inactivated during the high-temperature pelleting process. In addition, it needs to have high catalytic activity in animal body temperature (~40 °C) to achieve effective plant resistance hydrolysis of feed. In addition, the biomass degradation process needs to maintain high temperature to ensure maximum destruction of biomass to facilitate better enzymatic performance. However, this process has high cost and environmental pressure, as it requires high-level equipment and continuous energy supply [23]. Consequently, improving the thermostability of the enzyme and the catalytic activity of the enzyme at low temperatures causes rapid degradation of biomass at low temperatures, which greatly reduces production costs and environmental pollution.

The enzyme kinetic parameters were determined using beechwood xylan as the substrate at 40 °C. The graphs indicating the equations derived from the Lineweaver and Burk regression plots, used to calculate the kinetic parameters of each enzyme, are included in the supplementary materials (Fig. S3). As shown in Table 1, compared with the WT, the K_m values of mutants N207G and MF53/54SL+N207G were reduced (0.85 and 0.83 vs 0.96 mg/mL), indicating that the binding force of the two mutants to the substrate was slightly enhanced. However, the K_m value of mutant MF53/54SL increased (1.30 vs 0.96 mg/mL). Generally, the value of K_m does not undergo significant changes. Notably, the product release rate (k_{cat}) of the three mutants was higher than that of the WT (1090, 1110, and 1260 vs. 530 s^{-1}), which suggested that all mutants were superior to the WT in terms of substrate turnover number. Consequently, the catalytic efficiency (k_{cat}/K_m) of the two mutants and their combination have also greatly improved (1.9–2.8 fold; 1050, 1300, and 1530 vs. 550 μmol/min·mg) compared to that of WT, and the catalytic efficiency of the combined mutant MF53/54SL+N207G exceeded 1500 mL/s·mg, which was mainly due to the enhanced binding force of the enzyme and the substrate and the faster release of the product. In addition, compared with the WT XYL10C_ΔN, all mutants showed improved specific activities (1.9- to 2.9-fold; 1990, 1370, and 2090 vs. 710 U/mg), and the specific activity of the mutant MF53/54SL+N207G exceeded 2000 U/mg, which is higher than that of xylanases from *Bacillus* [24], *Aspergillus aculeatus*, and *Aspergillus niger* [25] at the same temperature. The same trends in specific activity and catalytic efficiency were observed when sugarcane xylan and corn cob xylan were used as substrates. For example, as shown in Table 2, the specific activity and catalytic efficiency of the three mutants were 1.5-2.8 times (1940, 1120, and 2080 vs 740 U/mg) and 1.3-3.4 times (750, 400, and 1100 vs 320 μmol/min·mg) higher than that of the WT, when sugarcane xylan was used as the substrate. When corncob xylan was used as the substrate, the specific activity and catalytic efficiency of the mutants were 3-5 times (1980, 1370, and 2080 vs. 770 U/mg) and 0.8-1.7 times (830, 530, and 1290 vs 300 μmol/min·mg) higher than that of the WT. The catalytic activity of most GH10 xylanases at 40 °C has not yet been studied. These findings additionally demonstrate that the strategies used in this study can enhance low-temperature catalytic activities.

The kinetic parameters and specific activity of all enzymes under their optimal conditions (85–90 °C and pH 4.0–4.5) were also determined with beechwood xylan as the substrate. All the graphs with Lineweaver and Burk regression and the equation that was used to calculate kinetic parameters of each enzyme under their optimal conditions are included in the supplementary materials (Fig. S4). As shown in Table S2, the catalytic efficiency of the mutants MF53/54SL and MF53/54SL+N207G was comparable to that of WT XYL10C_ΔN (5890 and 7440 vs. 7110 mL/s·mg), but the catalytic efficiency of mutant N207G was significantly higher than that of the WT XYL10C_ΔN (1.7-fold; 11750 vs. 7110 mL/s·mg). In addition, compared with the WT XYL10C_ΔN, all mutants showed improved specific activities (1.2- to 1.4-fold; 10740, 11390, and 11990 vs. 8770 U/mg) under the optimal conditions. The results indicate that amino acid mutations at the same position have different effects on enzyme catalytic kinetics under different temperature conditions. The mutation sites in this study had a greater impact on the catalytic kinetics of the enzyme at lower temperatures.

Thermostability assays of WT and mutants

Natural xylanase usually has limited application in the industry owing to its poor thermal stability and limited catalytic activity [26]. Rational design via site-specific mutagenesis and directed evolution are useful for improving the enzymatic performance and for reducing these limitations to meet industrial requirements [27]. Generally, the thermal stability of an enzyme corresponds to the rigidity of the protein structure. The stronger the rigidity, the more heat-resistant the enzyme is. The flexibility of the enzyme catalytic center corresponds to the catalytic efficiency, and the more flexible the catalytic efficiency [28]. It is a challenge to design enzyme molecules to enhance the catalytic performance of enzymes while maintaining or improving the original level of thermal stability.

As shown in Fig. 2D, after the incubation of WT XYL10C_ΔN at 85 °C for 0.5 h, the residual activity decreased to 56.0%. In contrast, the mutants MF53/54SL and MF53/54SL+N207G showed improved thermostability, retaining 81.6% and 74.4% of their maximal activity, respectively. As shown in Fig. 2E, after treatment at 90 °C for 10 min, the MF53/54SL and MF53/54SL+N207G had 80% and 70% of the maximal activity respectively, which were higher than those of the WT (67%). The thermostability of N207G was slightly lower than that of the WT, but more than 65% of the enzyme activity remained after treatment at 90 °C for 5 min. As shown in the figure, the thermal stability of all enzymes followed the order of MF53/54SL > MF53/54SL+N207G >XYL10C_ΔN > N207G. Commercial xylanases should be highly effective, resist various extreme environments, and have high expression efficiency to suit industrial requirements. For instance, the manufacture of animal feed requires enzymes to withstand short-heat treatment (~90 °C) during the pelleting process and to have high catalytic activity at lower temperatures (~40 °C). The pulp industry requires enzymes that can perform efficiently under alkaline and high-temperature conditions. In general, these three mutants roughly meet such industrial requirements [9].

The half-life ($t_{1/2}$) at high temperatures is an important parameter that indicates the thermostability of enzymes. As shown in Fig. 2E, the $t_{1/2}$ values of WT, MF53/54SL, N207G, and MF53/54SL+N207G at 90 °C and 85 °C were 42, 75, 16, and 50 min and 7, 17, 5, and 14 min, respectively (Table 3). The mutants MF53/54SL and MF53/54SL+N207G performed better than the WT in terms of thermostability, with $t_{1/2}$ increasing up to ~1.2 -1.8folds at 85 °C and ~2.0 - 2.4 folds at 90 °C, respectively. Hence, MF53/54SL is the best in terms of improved thermostability. The thermal stability of these two mutants was significantly better than that of other GH10 xylanases, such as 4F8X from *Penicillium canescens*, which lost 80% of its initial activity after incubation at 70 °C for 15 min [29], and the thermostability of mutants XynAS9_T from *Aspergillus fumigatus,* which retained only 50% of its initial activity at 75 °C for 40 min [30].

The estimation of T_m and T_{50} is also a reliable method for investigating the thermal stability of enzymes. As demonstrated in Fig. 2F, the T_m values of the WT and its mutants were investigated at a temperature profile of 40–120 °C. Compared to the T_m of XYL10C_ΔN (73.3 °C), the T_m values of mutants MF53/54SL and MF53/54SL+N207G showed an increase of ~7.7 °C (81.0 °C) and 6.4 °C (79.7 °C),

respectively (Table 3). Compared to the T_{50} of XYL10C_ΔN (85.5 °C), the mutants MF53/54SL and MF53/54SL+N207G showed an increase of ~3.5 °C (89.0 °C) and 3.0 °C (88.5 °C). However, compared with the WT, the T_m and T_{50} values of the mutant N207G were reduced by ~3.1 °C and ~2.0 °C, respectively. The thermostability of the mutants was generally superior to most GH10 xylanases derived from fungi, such as the enzyme from *Fusarium oxysporum*, which shows approximately 73% residual activity after incubation at 50 °C for 60 min [31], and the enzyme from *Thermoascus aurantiacus* which shows approximately 50% residual activity after incubation at 71 °C for 30 min [32]. The flexible loop of GH10 xylanases plays a vital role in thermostability [8, 33]. For instance, the introduction of a disulfide bond elevated the Tm value of xylanase TLX from 66 °C to 74 °C [34], and XYNII from T*richoderma reesei* had increased the thermostability by 11 °C [35]. This implies that the covalent interaction between the loop sequence and the TIM-barral region is significant for enhancing thermostability. These data support that residue substitutions at sites 53 and 54 make the most outstanding contributions to thermostability improvement. The excellent thermal stability under high temperature makes xylanase more suitable for applications in the feed, food, biofuel, and biotransformation industries. These results also indicate that the combinatorial mutant MF53/54SL+N207G had higher activity at lower temperatures and maintained more residual activity after high-temperature treatment.

Improved thermostability and catalytic performance explored by MD simulations

MD simulations of WT and its three mutants were performed for 30 ns at 313 K. As represented by the RMSD of the protein backbone relative to the initial conformation, all systems reached a dynamic equilibrium state after the first 10 ns of the simulation. Generally, the overall RMSD of the enzyme structure was reduced, making it rigid, thereby increasing its thermostability [36]. Compared with WT XYL10C_ΔN, the mutants, MF53/54SL and MF53/54SL+N207G, displayed enhanced rigidity of the conformation, with lower RMSD values at 313 K. However, the mutant N207G showed improved flexibility (Fig. 3A). Therefore, MF53/54SL and MF53/54SL+N207G were thermally more stable compared to WT. Moreover, as shown in Fig. 3B, the plasticity of all mutants was measured by root mean square fluctuations (RMSF) analysis compared with the WT XYL10C_ΔN through independent trajectory calculations. Some regions, especially the loops between α-helices and β-sheets, showed significant differences in conformational fluctuations. For instance, the 53rd and 54th mutations enhanced the rigidity of loop2 (residues 48–64), thereby enhancing the thermal stability of the protein. The N207G mutation mainly increased the flexibility of loop3 (residues 85–105) and loop4 (residues 133–156), thereby reducing the stability of the protein. “Rg” stands for the radius of rotation, which mainly measures the degree of expansion and compression of the protein system. The smaller the radius, the smaller the expansion and the more stable the protein [37]. The overall structures of MF53/54SL and MF53/54SL+N207G were tighter than the WT, and the mutant N207G was slightly swollen compared to the WT (Fig. 3C). The results of the simulations were consistent with the trend of the experimental data, indicating that the thermostability of the two mutants was significantly improved.

As shown in Fig. 4, after molecular docking, it was observed that when Met53/54Phe was mutated to Ser/Leu, the side chains of the two amino acids extended into the catalytic channel and interacted with

multiple key substrate-binding sites in the catalytic channel. On one hand, both HG and H atoms in the side chain of Ser53 can form hydrogen bond interactions with the O atom of Glu90, where the side chain can interact with the substrate-binding site Lys50 and the substrate molecule. On the other hand, the H atom of Leu54 and the atoms HG1 and H of the neighboring amino acid Thr55 with the atom O of the substrate-binding site Lys50 forms three pairs of hydrogen bonds. Previous studies have shown that Lys50 is a key amino acid site involved in substrate binding, and it forms a sterically stable network with Glu175, active site Glu135, and substrate molecules. The formation of this hydrogen bonding network makes the substrate molecules more tightly fixed in the catalytic channel, which is conducive to the interaction between the substrate molecules and the catalytic residues, and it ultimately increases the proton transfer rate and thus the catalytic efficiency. Third, Ser and Leu stabilized the conformation of the adjacent amino acids, Asn48 and Thr55, thereby stabilizing the conformation of the substrate-binding site Asp20, which is the key amino acid site at the exit of the catalytic channel thereby ensuring the normal release of the product. Briefly, when Met53/54Phe is mutated to Ser/Leu, the conformation of loop2 becomes more stable, which provides a structural basis for the binding of substrate molecules in the catalytic channel and the breaking of chemical bonds.

Hydrolysis of various lignocellulosic substrates with cellulase and xylanase

In the past two decades, the use of agricultural residual lignocellulosic biomass to produce bioethanol as a sustainable alternative to fossil fuels has received widespread attention. Owing to their superior richness and considerable sugar content, corn stalk, wheat bran, and corn cob are considered as ideal substrates for biorefining. However, owing to the complexity of plant cell wall structures, pretreatments such as alkali treatment and multi-enzyme synergistic reactions have become indispensable to accelerate the degradation of lignocellulosic biomass and ensure sustainable production of bioethanol. Pretreatment can partially eliminate the lignin bonds in the lignocellulose composite components, so that xylanase can easily hydrolyze xylan [38]. Naturally, the cellulose in the solid cell walls of plants is highly cross-linked with xylan through diferulic bridges. Consequently, the contact between cellulase and cellulose fibrils is limited, resulting in a decrease in cellulose hydrolysis activity, which in turn limits the downstream enzymatic hydrolysis process of other lignin components [39]. However, hemicellulose is an ideal raw material for biomass conversion. By adding auxiliary enzymes, especially xylanase, the hindrance of hemicellulose is eliminated so that cellulose is easily degraded by cellulase and, consecutively, more reducing sugars are produced. Therefore, the degradation of the complex structure of lignocellulose by the synergistic combination of xylanase and cellulase has become an attractive method. Research on the combined use of multiple commercial enzymes has shown that there is synergy between cellulase and xylanase [39]. Selig demonstrated that the addition of xylanase or other auxiliary enzymes (e.g., ferulic acid esterase and acetylxylan esterase) to cellobiohydrolase significantly increases the depolymerization of pretreated corn stover [40].

In this study, xylanase (XYL10C_ΔN and its mutant MF53/54SL+N207G) and cellulase were individually or simultaneously added to alkali-pretreated corn stalk, wheat bran, and corn cob to assess the generation of reducing sugars. Regardless of the enzyme components used to treat the three biomasses,

the amount of reducing sugars produced gradually increased with time to a stable plateau (Fig. 5). When the mutant MF53/54SL+N207G hydrolyzed the three substrates individually, sugar production reached the highest at 4, 2, and 3 h at 0.65, 6.7, and 3.4 μmol/mL, respectively, which was not significantly different from the WT XYL10C_ΔN (Fig. 5A, 5C, and 5E). Reducing sugar production reached the highest of 3.2, 18.5, and 7.7 μmol/mL at 6, 7, and 10 h, respectively, when the cellulase alone processed the three substrates. When cellulase with the mutant MF53/54SL+N207G synergistically hydrolyzed the three substrates, the sugar production reached the highest values of 5.4, 24.3, and 11.0 μmol/mL at 6, 7, and 4 h, respectively. Compared with the WT co-treatment group, the time to reach the maximum was 1, 2, and 3 h earlier. By comparing the rate of production in the first 2 h, the reducing sugar production rate of the mutant co-treatment group was 45%, 24%, and 31% higher than that of the WT co-treatment group. In addition, the maximum sugar yield of the mutant co-treatment group was 59, 35, and 40% higher than that of the cellulase-alone treatment group, and it was 8.0 times, 2.7 times, and 1.9 times higher than that of the xylanase treatment group.

The detailed synergistic effects of xylanase on cellulose-mediated hydrolysis of biomass were determined by DS values (Fig. 5B, 5D, and 5F). By definition, the amount of reducing sugars produced from the addition of xylanase to cellulase is related to a larger DS. Large amounts of reducing sugars were produced by the addition of xylanase to cellulase. The DS of the mutant cooperative treatment group reached the highest values of 1.9, 1.4, and 1.6, at 2, 3, and 1 h, respectively, which were 27%, 27%, and 14% higher than those of the WT cooperative treatment group. These results indicate that xylanase mutants promoted cellulase-catalyzed hydrolysis of these three types of biomass, and the order of strength was MF53/54SL+N207G > XYL10C_ΔN. Previous studies have reported that xylanase can significantly promote cellulase degradation in bagasse. During the alkaline pretreatment of bagasse hydrolysis, endoxylanase Xyn11A and endoglucanase Cel7B had a high synergistic effect (6.3), which significantly increased sugar production [41]. Therefore, the type of substrate and the pretreatment method used may affect the synergistic effect between xylanase and cellulase.

Meanwhile, from Fig. 6, it can be seen that the analysis of the changes in the dry matter quality of the three substrates after hydrolysis showed that the dry matter reduction in the mutant cooperative treatment group was 0.64 g, 0.83 g, and 0.76 g after 24 h, accounting for 32, 55, and 51% of the total dry matter weight, respectively. In comparison to the cellulase-alone treatment group and xylanase-alone treatment group, it increased by 60%, 51%, and 58% and 3, 1.1 times, and 1.5, respectively, and there was no significant difference compared with the WT co-treatment group.

SEM

SEM was used to observe the alterations in the surface structure of corn stalk, wheat bran, and corn cob after various enzyme treatments. Fig. S5 in the supplementary materials shows the surface structures of all three substrates after 24 h of buffer treatment. The results show that the different plant-derived biomasses have a huge difference in surface structure due to the different proportions of cellulose, hemicellulose, lignin, and other main components or due to the different degrees of cross-linking. As

shown in Fig. 7, xylanase treatment of the three substrates significantly changed the surface structure of the biomass. Numerous holes appeared on the surface of the corn stalks, and they continued to enlarge (Fig. 7A). The cell wall structure on the surface of the bran was destroyed, and the usual boundaries between the cells disappeared (Fig. 7D). First, corn cob hydrolyzed on the inside, and numerous holes appeared (Fig. 7G). In comparison, cellulase-alone treatment resulted in a more serious damage to the surface of the biomass, such as deeper peeling between fibers, more severe fiber fragments, and larger holes. However, the cellulose is covered by hemicellulose and tightly interwoven with other components and cannot be further degraded (Fig. 7B, 7E, and 7H). When xylanase and cellulase synergistically hydrolyze the three substrates, the degree of damage to the surface of the biomass increased, the interweaving state of each component completely separated, and the pores disappeared completely. Moreover, the degree of adhesion of cellulose to hemicellulose was reduced (Fig. 7C, 7F, and 7I). The cross-linking between cellulose and hemicellulose forms a complex network arrangement. Xylanase may destroy the original network structure of lignocellulose, thereby increasing the degree of swelling and porosity. Xylanase, as an auxiliary enzyme, ravages the physical structure of lignocellulose to promote cellulase to penetrate the microfibrous pores of cellulose and more easily bind to cellulose, thereby accelerating the hydrolysis of the substrate and improving the production of reducing sugar [42]. This synergistic effect of xylanase is a reliable solution to overcome the obstacles in the saccharification reaction, and to finally obtain the maximum amount of reducing sugar by adding the least amount of enzyme to the lignocellulose substrate.

Conclusions

The high catalytic efficiency and excellent thermal stability of xylanase are the key characteristics of xylanase used in the production of biomass degradation raw materials for the production of bioethanol. In this study, protein engineering technology was used to generate various mutants of xylanase, and their suitability for industrial applications was evaluated. A novel characteristic of the constructed mutant MF53/54SL + N207G is the simultaneous improvement of thermal stability and low-temperature catalytic efficiency, which is invaluable in protein engineering. These results provide useful insights regarding the relationship between the structure and function of xylanase.

Materials And Methods

Materials

The gene coding objective-engineered xylanase (wild-type [WT] XYL10C_ΔN, GenBank accession number FJ492963) with codon optimization was synthesized by Qingke Biotechnology (Nanjing, China). Competent cells of *Escherichia coli* Trans1-T1 purchased from Tiangen (Nanjing, China) were used for plasmid DNA amplification. Vector pPIC9k and *Pichia pastoris* GS115 were purchased from Invitrogen (Carlsbad, CA, USA) and used for recombinant enzyme expression. FastPfu DNA polymerase, a Fast Mutagenesis System Kit, and restriction endonucleases (*E*coRI, *N*otI, and *B*glII) were procured from Vazyme (Nanjing, China). Standards and beechwood xylan were purchased from Sigma-Aldrich (St.

Louis, MO, USA). Wheat bran, corn stalk, and corn cob were collected from farmlands in the Jingkou District of Zhenjiang City. All other reagents were of analytical grade and were commercially available.

Selection of the mutation site and site-directed mutagenesis

Loop2 of XYL10C_ΔN is located around the catalytic channel, and the component residue 52-FMFT-55 in loop2 forms a unique helical structure (Fig. 1). Multiple sequence alignments of fungal xylanases of GH10 were conducted using FASTA [43] and ClustalW algorithms [44]. Following conformational and sequence scrutiny of loop2, two key locations related to XYL10C_ΔN functionality were identified and selected for mutagenesis. The mutants were first constructed using the Fast Mutagenesis System Kit (TransGen) with recombinant plasmids pPIC9-XYL10C_ΔN as the templates for preliminary screening. All primers used in this study are listed in the Additional File 1 (Table S3).

Protein expression and purification

After verification of DNA sequencing, linearization of the recombinant plasmid was achieved by using restriction endonucleases *Bgl*II, and it was further electroporated to transform *P. pastoris* GS115 host cells for recombinant gene expression. Screening of the positive transformants was conducted based on the "enzymatic activities of the enzyme" in shake tubes as described by Yuo et al. [11], and the transformant with the highest xylanase activity at 40 °C was selected for fermentation. The transformants selected were precultured on yeast extract peptone dextrose ([YPD], 30 mL, 1% yeast extract, 2% tryptone, and 2% glucose) media overnight at 30 °C by shaking at 220 rpm and cultured for protein expression in a buffered glycerol-complex medium (BMGY; 300 mL, 1% glycerol, 2% tryptone, 1.34% yeast nitrogen base [YNB], and 4 mg/mL biotin) in a 1-L flask at 30 °C by shaking at 220 rpm for 48 h. The expression was then induced by transferring the cells into a buffered methanol-complex medium (BMMY; 200 mL, 2% tryptone, 1.34% YNB, 4 mg/mL biotin, 1% carbinol) in a 1-L flask at 30 °C and 220 rpm in a shaking incubator for 48 h. During the induction process, the medium was supplemented with 1% (v/v) carbinol every 12 h.

To separate and collect the crude protein supernatant, the fermentation broth was centrifuged at 12,000 × g for 10 min. The ammonium sulfate precipitation method was used to concentrate the sample to 10 mL, dialyzed, and desalted in 20 mM McIlvaine buffer (pH 6.5) overnight. The desalted sample was then loaded onto a HiTrap SP HP 5-mL FPLC column (GE Healthcare) pre-equilibrated with a buffer. Finally, the target protein was eluted using a linear gradient solution of NaCl (0–1.0 M) in the same buffer. Sodium dodecyl sulfate–polyacrylamide gel electrophoresis (SDS–PAGE) was used to determine the purity of the target protein. For the estimation of protein concentration, the Bradford assay with bovine serum albumin was employed as the standard.

Enzymatic properties determination

The 3,5-Dinitrosalicylic acid (DNS) method was used to detect reducing sugar release [45]. The amount of enzyme required to release 1 μmol of reducing sugar per minute under the test conditions was defined as

one unit of enzyme activity (U). Glycine-HCl (100 mM, pH 1.0–2.5), citric acid-Na_2HPO_4 (200 mM, pH 2.5–8.0), and glycine-NaOH (100 mM, pH 8.0–11.0) were used to measure pH adaptability and stability profiles. The optimal pH for enzymes were identified at 85 °C for 10 min at pH 1.0–9.0. The pH stability of enzymes was evaluated by pre-incubating the enzyme at 37 °C for 1 h without substrate, followed by determination of the residual activities at pH 4.0, and 85 °C.

Accordingly, the following four factors were used to compare the thermal properties of the enzymes: the temperature corresponding to the maximum enzyme activity (T_{max}), half-life ($t_{1/2}$) of the enzyme at a specific temperature, temperature corresponding to the remaining 50% of the maximum activity after 30 min of treatment (T_{50}), and temperature corresponding to half of the protein structure denaturation (T_m). The T_{max} values for all enzymes were measured in the temperature range of 40–95 °C at the optimum pH for 10 min. The $t_{1/2}$ values of the enzyme activity were measured residually under optimal conditions of pH and temperature after incubation at 85 °C or 90 °C without substrate at a concentration of approximately 50 μg/mL. In the absence of substrate, the T_{50} values were determined after incubating the enzyme (approximately 50 μg/mL) for 0.5 h at the specified range of temperature, between 75 and 95 °C. The melting temperature (T_m) of the enzymes was assessed using a MicroCal™ VP-Capil-lary differential scanning calorimetry apparatus (GE Healthcare, Sweden) in 0.5 mL of 20-mM McIlvaine buffer (pH 6.5) at a concentration of approximately 0.2 mg/mL. After the protein and control were degassed, they were heat-treated in the range of 30–110 °C at a heating rate of 2 °C/min. All reactions were conducted and analyzed in triplicate.

The kinetic parameters (K_m, V_{max}, and k_{cat}) of all the purified enzymes were measured under low temperature (40 °C, optimal pH, and 5 min) and their optimal conditions in a 100 mM McIlvaine buffer containing beechwood xylan, sugarcane xylan, and corncob xylan with a concentration of 0.5 mg/mL as the substrate. GraphPad Prism (version 5.01; La Jolla, CA, USA) with the Michaelis–Menten model was used to calculate the kinetic parameters. All the tests and calculations were repeated three times.

Molecular docking and MD simulation

To analyze the changes in the interaction between the enzyme and the substrate after mutation, the WT and its mutants were docked with xylopentaose using the AutoDock Vina program for theoretical rigid docking [46]. The docked enzyme-substrate complex underwent energy optimization and conformational screening. Molecular dynamic simulation (MD) was performed (313 K, 30 ns) using the Amber 14 package. The force field ff99SB was used to describe the system [47]. The root mean square deviation (RMSD) was assessed using minimum squares fitting of the protein backbone molecules. The first 20 ns simulation was used for the stabilization of the system, and the last 10 ns trajectory information was used for the dynamic simulation analysis. Three-dimensional visualization and graphic preparation of protein molecules were completed using PyMOL version 1.7.2.1.

Enzymatic hydrolysis of lignocellulosic biomass

Corn stalk, wheat bran, and corn cob were soaked in 15% (w/w) aqueous ammonia (SAA) at 60°C for 24 h, as previously described [11]. Three lignocellulose biomass samples were soaked in 30 mL phosphate buffer (pH 4.5, 0.01 mM) at a concentration of 5% (w/v), followed by the addition of cellulase from *Aspergillus niger* [48] and/or xylanases. Subsequently, 30 mL of the reaction system was placed in a 50 mL Erlenmeyer flask and incubated at 40°C with shaking at 220 rpm for 24 h. Experiments were divided into five sets and conducted in parallel, including cellulase (50U)-added group, xylanase (50U)-added group, both cellulase (50U) and xylanase (50U), including the WT and mutant groups, and a control group. The buffer volume loadings of the control group were the same as those of the experimental group. During the enzymatic hydrolysis, the samples (0.8 mL) were collected in 1.5 mL Eppendorf tubes at regular intervals (1 h). The supernatant was obtained from the mixture after centrifugation at 12,00 rpm for 5min and subjected to further analysis. Triplicate experiments were performed in parallel.

The amount of reducing sugar produced in the supernatant of the reaction system was calculated using the following Lambert–Beer law formula:

$$C = \frac{A}{\epsilon L} \quad (1)$$

where A is the absorbance and ϵL is the slope developed from the xylose standard curve. The degree of synergy (DS) was analyzed according to the following equation:

$$DS = \frac{Y_{1+2}}{Y_1 + Y_2} \quad (2)$$

Where Y_{1+2} represents the content of reducing sugars produced in the reaction system when xylanase and cellulase were added simultaneously. Y_1 and Y_2 represent the amount of reducing sugar when cellulase and xylanase are added during the hydrolysis process, respectively [11].

The data obtained from this experiment were analyzed using SPSS 17.0, one-way analysis of variance (ANOVA), and Origin Pro 9 for statistical analysis.

Scanning electron microscope (SEM) analysis

After the reaction was complete, the insoluble precipitate was collected. The soluble components were removed by washing it thrice with deionized water, followed by drying at 60 °C. Finally, after sputtering gold plating on the dried sample, an SEM was used to observe the changes in the surface structure of the sample at 300-400x magnification.

Abbreviations

BMGY: buffered glycerol-complex medium; BMMY: buffered methanol-complex medium; CD: circular dichroism; DNS: 3,5-dinitrosalicylic acid; DS: degree of synergy; DSC: differential scanning calorimetry; GH: glycoside hydrolase; MD: molecular dynamics; RMSD: root mean square deviation; RMSF: root mean

square fluctuation; SDS–PAGE: sodium dodecyl sulfate–polyacrylamide gel electrophoresis; SEM: scanning electron microscope; YNB: yeast nitrogen base W/O amino acids; YPD: yeast extract peptone dextrose.

Declarations

Ethical approval and consent to participate

Not applicable.

Consent for publication

All authors consent the manuscript for publication in Biotechnology for Biofuels.

Authors' contributions

SY performed the major experiments including the construction of mutants and enzyme characterization, and drafted the manuscript; ZZ, WZ, ZB and YH participated in enzyme activity assay; ZC, JW, and XW participated in the discussion; JW and ZC performed data analysis and guided the experiment. JL and YC polished the language of the article. JW and HL were the corresponding authors; they designed the study, supervised the work and analyzed the experimental data. All authors reviewed the results and approved the final version of the manuscript.

Author details

[1] School of Biotechnology, Jiangsu University of Science and Technology, Zhenjiang 212018, P R China;

[2] Sericultural Research Institute, Chinese Academy of Agricultural Sciences, Zhenjiang 212018, P R China;

[3] Department of Nephrology, Affiliated Hospital of Jiangsu University, Zhenjiang 212001, P R China;

[4] Xinyuan cocoon silk group co., ltd., Nantong 226600, P R China;

[5] Institute of Animal Sciences, Chinese Academy of Agricultural Sciences, Beijing 100081, China.

Acknowledgments

Not applicable.

Competing interests

The authors declare that they have no competing interests.

Availability of data and materials

The dataset supporting the conclusions of this article are included within the article (and its Additional files 1 and 2).

Funding

The authors would like to thank the financial support from the Natural Science Foundation of Jiangsu Province (BK20190957), the National Natural Science Foundation of China (Grant Number 21978121), the National Natural Science Foundation of China (Grant Number 31472127), and the Editage for helping us to polish the language of the article.

References

1. Rjesson B. PL. Good or bad bioethanol from a greenhouse gas perspective–what determines this? Appl Energ. 2009;86(5):589–94.
2. Teeravivattanakit T, Baramee S, Phitsuwan P, Sornyotha S, Waeonukul R, Pason P, Tachaapaikoon C, Poomputsa K, Kosugi A, Sakka K, Ratanakhanokchai K. Chemical pretreatment-independent saccharifications of xylan and cellulose of rice straw by bacterial weak lignin-binding xylanolytic and cellulolytic enzymes. Appl Environ Microb. 2017;83(22):1517–22.
3. Nguyen STC, Freund HL, Kasanjian J, Berlemont R. Function, distribution, and annotation of characterized cellulases, xylanases, and chitinases from CAZy. Appl Microbiol Biot. 2018;102(4):1629–37.
4. Gottumukkala LD, Haigh K, Görgens J. Trends and advances in conversion of lignocellulosic biomass to biobutanol: microbes, bioprocesses and industrial viability. Renewable Sustainable Energy Rev. 2017;76:963–73.
5. Igarashi K. Traffic jams reduce hydrolytic efficiency of cellulase on cellulose surface. Science. 2011;334(6055):453.
6. Bajaj P, Mahajan R. Cellulase and xylanase synergism in industrial biotechnology. Appl Microbiol Biot. 2019;103(11):8711–24.
7. Kumar V, Chhabra D, Shukla P. Xylanase production from *Thermomyces lanuginosus* VAPS-24 using low cost agro-industrial residues via hybrid optimization tools and its potential use for saccharification. Bioresource Technol. 2017;243:1009–19.
8. Yang J, Han Z. Understanding the positional binding and substrate interaction of a highly thermostable GH10 xylanase from *Thermotoga maritima* by molecular docking. Biomolecules. 2018;8(3):64.
9. Kumar V, Dangi AK, Shukla P. Engineering thermostable microbial xylanases toward its industrial applications. Mol Biotechnol. 2018;60(3):226–35.
10. Azouz RAM, Hegazy UM, Said MM, Bassuiny RI, Salem AM, Fahmy AS. Improving the catalytic efficiency of thermostable *Geobacillus stearothermophilus* xylanase XT6 by single-amino acid substitution. J Biochem. 2020;167(2):203–15.

11. You S, Xie C, Ma R, Huang H, Herman RA, Su X, Ge Y, Cai H, Yao B, Wang J, Luo H. Improvement in catalytic activity and thermostability of a GH10 xylanase and its synergistic degradation of biomass with cellulase. Biotechnol Biofuels. 2019;12(1):278.
12. You S, Chen C, Tu T, Wang X, Ma R, Cai H, Guo R, Luo H, Yao B. Insight into the functional roles of Glu175 in the hyperthermostable xylanase XYL10C-ΔN through structural analysis and site-saturation mutagenesis. Biotechnol Biofuels. 2018;11(1):;159.
13. Zhai X, Go MK, O'Donoghue AC, Amyes TL, Pegan SD, Wang Y, Loria JP, Mesecar AD, Richard JP. Enzyme architecture: the effect of replacement and deletion mutations of loop 6 on catalysis by triosephosphate isomerase. Biochemistry. 2014;53(21):3486–501.
14. Denisenko YA, Gusakov AV, Rozhkova AM, Osipov DO, Zorov IN, Matys VY, Uporov IV, Sinitsyn AP. Site-directed mutagenesis of GH10 xylanase A from *Penicillium canescens* for determining factors affecting the enzyme thermostability. Int J Biol Macromol. 2017;104:665–71.
15. Matsuzawa T, Kaneko S, Yaoi K. Improvement of thermostability and activity of T*richoderma reesei* endo-xylanase Xyn III on insoluble substrates. Appl Microbiol Biot. 2016;100(18):8043–51.
16. Zubieta MP, Gerhardt JA, Rubio MV, Terrasan CRF, Persinoti GF, Antoniel EP, Contesini FJ, Prade RA, Damasio A. Improvement of homologous GH10 xylanase production by deletion of genes with predicted function in the *Aspergillus nidulans* secretion pathway. Microb Biotechnol. 2020;13(4):1245–53.
17. Alokika SB. Production, characteristics, and biotechnological applications of microbial xylanases. 2019;103(21–22):8763–84.
18. Tony C, Charles G, Georges F. Xylanases, xylanase families and extremophilic xylanases. Fems Microbiol Rev. 2010;29(1):3–23.
19. Leggio LL, Kalogiannis S, Bhat MK, Pickersgill RW. High resolution structure and sequence of *T. aurantiacus* xylanase I: implications for the evolution of thermostability in family 10 xylanases and enzymes with (beta)alpha-barrel architecture. Proteins. 1999;36(3):295–306.
20. Xiong K, Xiong S, Gao S, Li Q, Sun B, Li X. Improving hydrolysis characteristics of xylanases by site-directed mutagenesis in binding-site subsites from *Streptomyces* L10608. Int J Mol Sci. 2018;19(3):834.
21. Wu X, Tian Z, Jiang X, Zhang Q, Wang L. Enhancement in catalytic activity of *Aspergillus niger* XynB by selective site-directed mutagenesis of active site amino acids. Appl Microbiol Biot. 2018;102(6):249–60.
22. Chadha BS, Kaur B, Basotra N, Tsang A, Pandey A. Thermostable xylanases from thermophilic fungi and bacteria: Current perspective. Bioresour Technol. 2019;277:195–203.
23. Bhatia SK, Jagtap SS, Bedekar AA, Bhatia RK, Patel AK, Pant D, Rajesh Banu J, Rao CV, Kim YG, Yang YH. Recent developments in pretreatment technologies on lignocellulosic biomass: effect of key parameters, technological improvements, and challenges. Bioresour Technol. 2020;300:122724.
24. Wang K, Cao R, Wang M, Lin Q, Zhan R, Xu H, Wang S. A novel thermostable GH10 xylanase with activities on a wide variety of cellulosic substrates from a xylanolytic *Bacillus* strain exhibiting

significant synergy with commercial celluclast 1.5 L in pretreated corn stover hydrolysis. Biotechnol Biofuels. 2019;12:48.

25. Uday USP, Majumdar R, Tiwari ON, Mishra U, Mondal A, Bandyopadhyay TK, Bhunia B. Isolation, screening and characterization of a novel extracellular xylanase from *Aspergillus niger* (KP874102.1) and its application in orange peel hydrolysis. Int J Biol Macromol. 2017;105(1):401–9.
26. Woodley JM. Integrating protein engineering with process design for biocatalysis. Philos Trans A Math Phys Eng Sci. 2018;376(2110):1364–503.
27. Lutz S, Iamurri SM. Protein Engineering: past, present, and future. Methods Mol Biol. 2018;1685:1–12.
28. Yu H, Dalby PA. Exploiting correlated molecular-dynamics networks to counteract enzyme activity-stability trade-off. P Natl Acad Sci U S A. 2018;115(52):12192–200.
29. Fedorova T, Chulkin A, Vavilova E, Maisuradze I, Trofimov A, Zorov I, Khotchenkov VP, Polyakov KM, Benevolensky SV, Koroleva OV, Lamzin VS. Purification, biochemical characterization, and structure of recombinant endo-1,4-β-xylanase XylE. Biochemistry. 2012;77(10):1190–8.
30. Li G, Chen X, Zhou X, Huang R, Zhang R. Improvement of GH10 family xylanase thermostability by introducing of an extra α-helix at the C-terminal. Biochem Bioph Res Co. 2019;515(3):417–22.
31. Dimarogona T, Christakopoulos, Chrysina ED. The structure of a GH10 xylanase from *Fusarium oxysporum* reveals the presence of an extended loop on top of the catalytic cleft. Acta Crystallogr D Biol Crystallogr. 2012;68(7):735–42.
32. Angelica R, Gabriela C, Letícia M, Roberto R, Fernanda C, Fernando AG, Jeffrey AM, Michael J, Eleni G. Roberto. Engineering increased thermostability in the GH-10 endo-1,4-β-xylanase from *Thermoascus aurantiacus* CBMAI 756. Int J Biol Macromol. 2016;93(1):20–6.
33. Al-Qahtani M, Ahiwe EU, Abdallh ME, Chang'A EP, Gausi H, Bedford MR, Iji PA. Endogenous enzyme activities and tibia bone development of broiler chickens fed wheat-based diets supplemented with xylanase, beta-glucanase and phytase. Asian Austral J Anim. 2020.
34. Wang Y, Fu Z, Huang H, Zhang H, Yao B, Xiong H, Turunen O. Improved thermal performance of Thermomyces lanuginosus GH11 xylanase by engineering of an N-terminal disulfide bridge. Bioresource Technol. 2012;112:275–9.
35. Fenel F, Leisola M, Janis J, Turunen O. A de novo designed N-terminal disulphide bridge stabilizes the *Trichoderma reesei* endo-1,4-β-xylanase II. J Biotechnol. 2004;108(2):137–43.
36. Chen J, Yu H, Liu C, Liu J, Shen Z. Improving stability of nitrile hydratase by bridging the salt-bridges in specific thermal-sensitive regions. J Biotechnol. 2013;164(2):354–62.
37. Rasouli S, Moghbeli MR, Nikkhah SJ. A deep insight into the polystyrene chain in cyclohexane at theta temperature: molecular dynamics simulation and quantum chemical calculations. J Mol Model. 2019;25(7):195.
38. Capolupo L, Faraco V. Green methods of lignocellulose pretreatment for biorefinery development. Appl Microbiol Biotechnol. 2016;100(22):9451–67.

39. Li J, Zhou P, Liu H, Xiong C, Liu Z. Synergism of cellulase, xylanase, and pectinase on hydrolyzing sugarcane bagasse resulting from different pretreatment technologies. Bioresource Technol. 2014;155:258–65.
40. Selig MJ, Knoshaug EP, Adney WS, Himmel ME, Decker SR. Synergistic enhancement of cellobiohydrolase performance on pretreated corn stover by addition of xylanase and esterase activities. Bioresource Technol. 2008;99(11):4997–5005.
41. Pavón-Orozco P, Santiago-Hernández A, Rosengren A, Hidalgo-Lara ME, St Lbrand H. The family II carbohydrate-binding module of xylanase CflXyn11A from *Cellulomonas flavigena* increases the synergy with cellulase TrCel7B from *Trichoderma reesei* during the hydrolysis of sugar cane bagasse. Bioresource Technol. 2012;104(1):622–30.
42. Hidayatullah IM, Setiadi T, Boopathy R, Kresnowati P. Xylanase inhibition by the derivatives of lignocellulosic material. Bioresour Technol. 2020;300:122740.
43. Pearson WR. Searching protein sequence libraries: comparison of the sensitivity and selectivity of the Smith-Waterman and FASTA algorithms. Genomics. 1991;11(3):635–50.
44. Thompson JD, Higgins DG, Gibson TJ. CLUSTAL W: improving the sensitivity of progressive multiple sequence alignment through sequence weighting, position-specific gap penalties and weight matrix choice. Nucleic Acids Res. 1994;22(22):4673–80.
45. McKee LS. Measuring enzyme kinetics of glycoside hydrolases using the 3,5-dinitrosalicylic acid assay. Methods Mol Biol. 2017;1588:27–36.
46. Trott O, Olson AJ. Software News and Update AutoDock Vina: improving the speed and accuracy of docking with a new scoring function, efficient optimization, and multithreading. J Comput Chem. 2010;31(2):455–61.
47. Lindorff-Larsen K, Piana S, Palmo K, Maragakis P, Klepeis JL, Dror RO, Shaw DE. Improved side-chain torsion potentials for the Amber ff99SB protein force field. Proteins. 2010;78(8):1950–58.
48. Moreau RA, Johnston DB, Powell MJ, Hicks KB. A comparison of commercial enzymes for the aqueous enzymatic extraction of corn oil from corn germ. J Am Oil Chem Soc. 2004;81(11):1071–75.

Tables

Table 1. Kinetic parameters and specific activity of XYL10C_ΔN and its three mutants at 40 °C[a].

	K_m (mg/mL)	k_{cat} (s^{-1})	V_{max} (μmol/min·mg)	k_{cat}/K_m (mL/s·mg)	Specific activity (U/mg)
XYL10C_ΔN	0.96 ± 0.18	530 ± 40	830 ± 62	550 ± 60	710 ± 45
MF53/54SL	1.30 ± 0.10	1090 ± 44	2140 ± 69	1050 ± 31	1990 ± 77
N207G	0.85 ± 0.01	1110 ± 6	1750 ± 9	1300 ± 11	1370 ± 64
MF53/54SL+N207G	0.83 ± 0.10	1260 ± 44	1980 ± 70	1530 ± 144	2090 ± 197

[a] beechwood xylan as substrate

Table 2 Kinetic parameters and specific activity of XYL10C_ΔN and its three mutants at 40 °C.

Substrate	Sugarcane xylan[a]				Corncob xylan[b]			
Enzymes	K_m (mg/mL)	V_{max} (μmol/min·mg)	k_{cat}/K_m (mL/s·mg)	Specific activity (U/mg)	K_m (mg/mL)	V_{max} (μmol/min·mg)	k_{cat}/K_m (mL/s·mg)	Specific activity (U/mg)
XYL10C_ΔN	1.52 ±0.04	730 ± 38	320 ± 28	740 ± 33	1.89 ± 0.14	810 ± 52	300 ± 15	770 ± 63
MF53/54SL	1.63 ± 0.17	1920 ± 81	750 ± 41	1940 ± 77	1.44 ± 0.16	1880 ± 88	830 ± 48	1980 ± 91
N207G	1.91 ± 0.08	1210 ± 56	400 ± 33	1120 ± 82	1.55 ± 0.11	1290 ± 72	530 ± 47	1370 ± 62
MF53/54SL+N207G	1.18 ± 0.10	2030 ± 79	1100 ± 81	2080 ± 85	1.03 ± 0.04	2090 ± 84	1290 ± 81	2080 ± 92

[a] Sugarcane xylan as substrate, [b] Corncob xylan as substrate.

Table 3. Half-lives of wild type and its mutants for thermal inactivation[a].

Enzyme	$t_{1/2}$ (min) at		T_{50} (°C)	T_m (°C)	ΔT_m (°C)
	85 °C	90 °C			
XYL10C_ΔN	42	7	85.5	73.3	
MF53/54SL	75	17	89	81.0	+ 7.7
N207G	16	5	83.5	70.2	− 3.1
MF53/54SL+N207G	50	14	88.5	79.7	+ 6.4

[a] The enzyme activity was assayed at each optimal conditions for 10 min.

Additional Files

Table S1. Comparison of the biochemical characterizations of mutants MF53/54SL and MF53/54SL+N207G with other xylanases.

Table S2. Kinetic parameters and specific activity of XYL10C_ΔN and its three mutants at optimal conditions.

Table S3. Primers used in this study.

Figure S1.Analysis of multiple sequences of GH10 Xylanases. The selected mutation sites are marked with red diamonds.

Figure S2. Sodium dodecylsulfate-polyacrylamide gel electrophoresis (SDS–PAGE) analysis of the purified XYL10C_ΔN and its mutants. Lanes: M, the standard protein molecular weight markers; **A, B, C,**

and **D**: XYL10C_ΔN, MF53/54SL, N207G, and MF53/54SL+N207G.

Figure S3. Graph with Lineweaver and Burk regression and the equation for enzymes at 40 °C. A. XYL10C_ΔN; **B.** MF53/54SL; **C.** N207G; **D.** MF53/54SL+N207G**.**

Figure S4. Graph with Lineweaver and Burk regression and the equation for enzymes at the optimum temperature. A. XYL10C_ΔN; **B.** MF53/54SL; **C.** N207G; **D.** MF53/54SL+N207G**.**

Figure S5. Surface structure of A. corn stalk, B. wheat bran, and C. corn cob treated with buffer for 24 h.

Figures

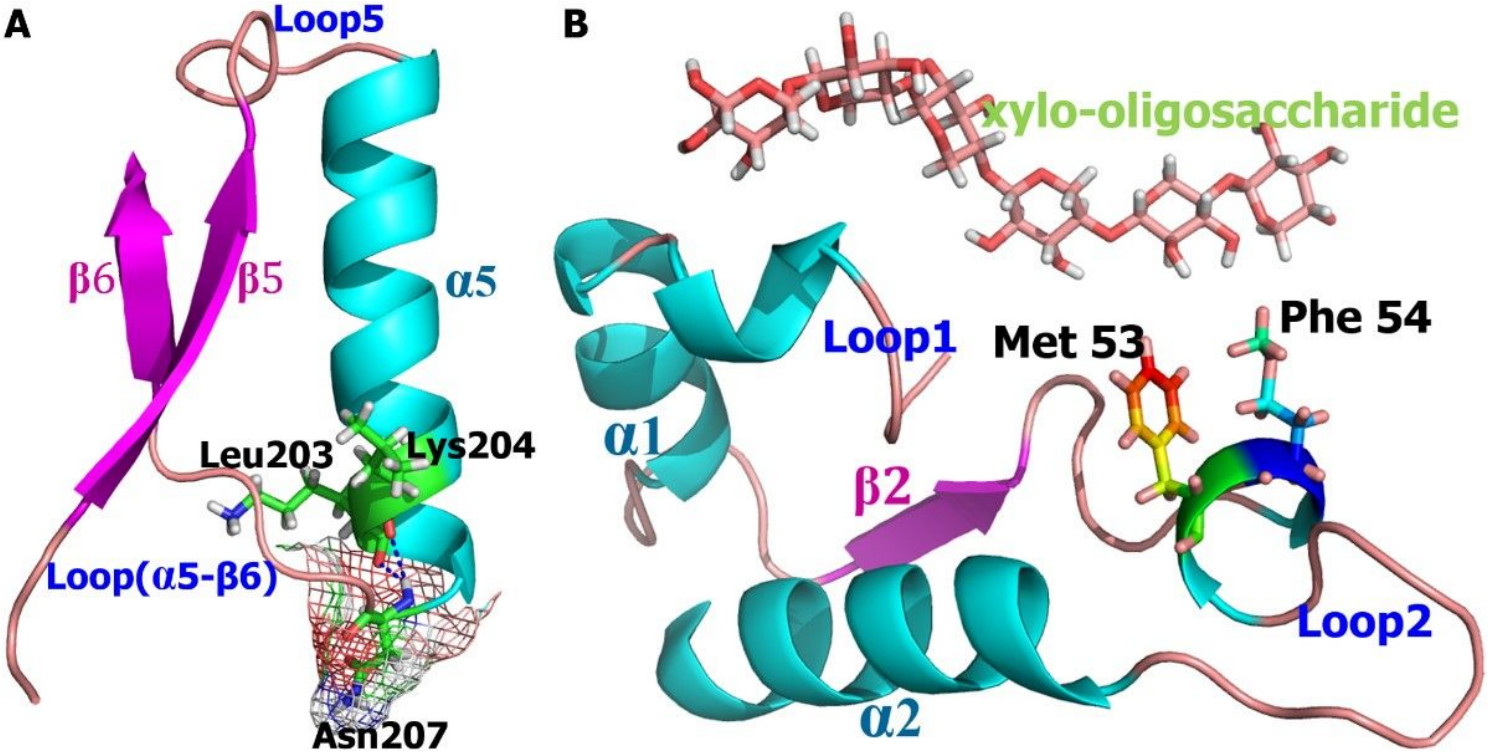

Figure 1

Selection of mutation sites. A. Location and configuration of Asn207; B. Location and configuration of Met53 and Phe54.

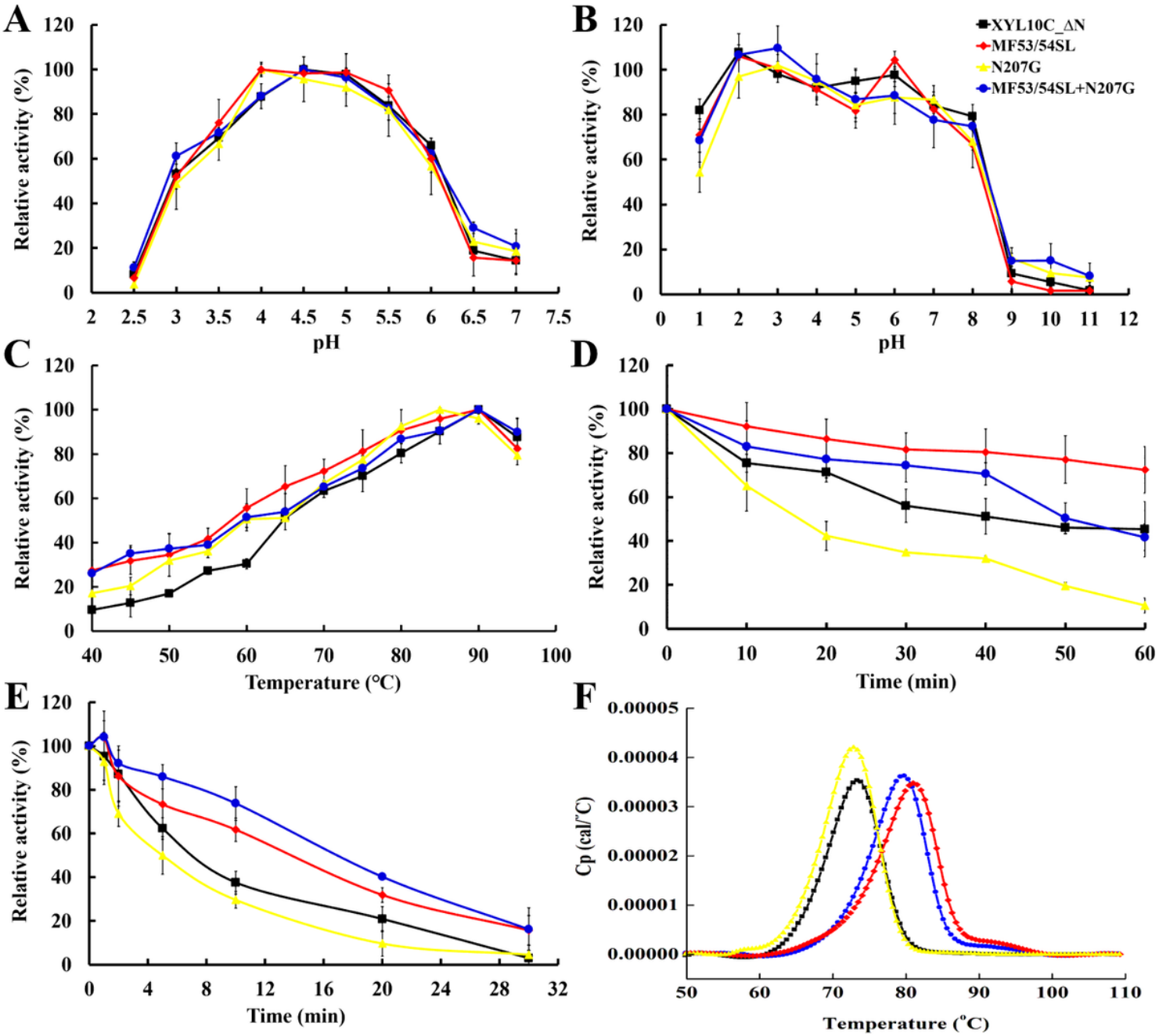

Figure 2

Enzyme properties of the purified recombinant wild-type XYL10C_ΔN and its mutants. A. pH-activity profiles of each enzyme tested at respective optimal temperatures; B. pH-stability profiles. After enzymes were incubated for 1 h at 37 °C in buffers ranging from pH 1.0 to 11.0, the residual activities were determined in 100 mM McIlvaine buffer at the optimal temperature and optimal pH of each enzyme; C. Temperature-activity profiles tested at the optimal pH of each enzyme; D. Temperature-stability profiles (t1/2) at 85°C; E. Half-lives of wild-type XYL10C_ΔN and its mutants at 90 °C; F. Thermograms determined by using differential scanning calorimetry (DSC). The calorimetric recordings for XYL10C_ΔN and its mutants were scanned at 1 °C/min in 10 mM phosphate buffered saline (PBS) (pH 6.5) at 350 μg/mL.

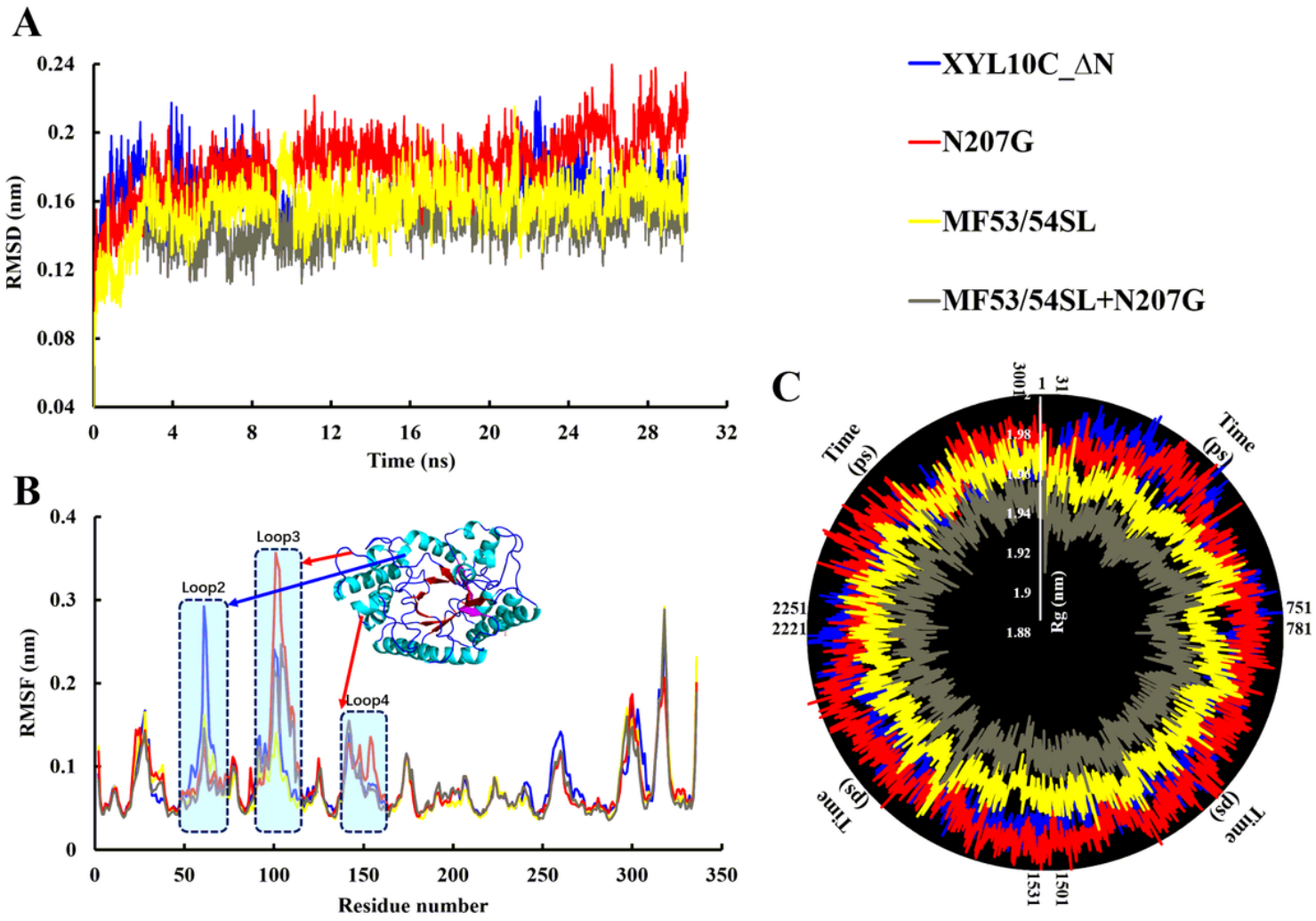

Figure 3

Molecular dynamics simulation analysis of thermal stability. A. Root mean square deviation (RMSD) values of the wild-type XYL10C_ΔN and its mutants. B. Root mean square fluctuations (RMSF) values during molecular dynamics (MD) simulation; C. Vibration deviation radius (Rg) of the wild-type XYL10C_ΔN and its mutants.

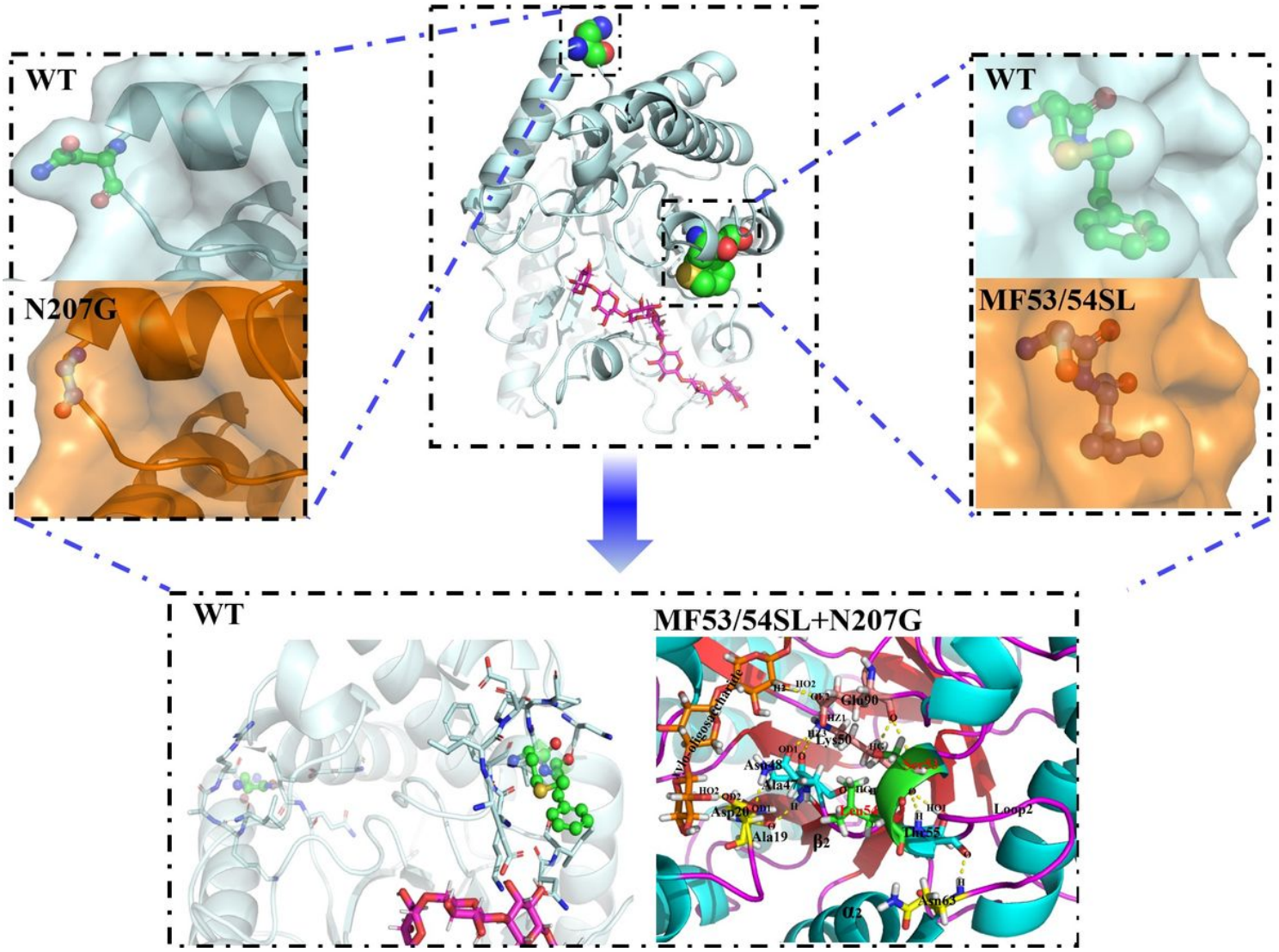

Figure 4

Location of the catalytic-increased mutations and the structural characteristics of the wild type and mutants.

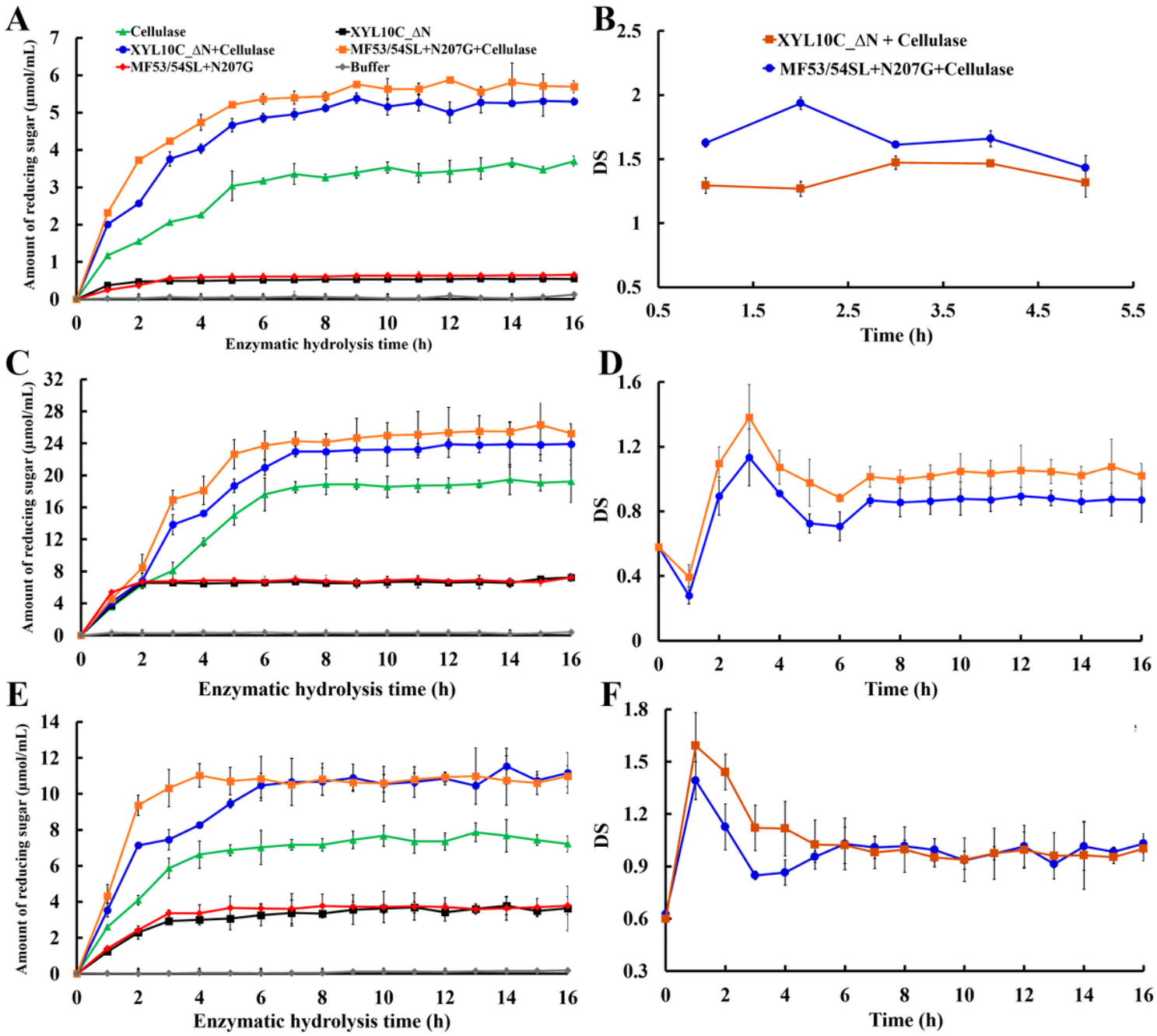

Figure 5

Time-course hydrolysis of corn stalk (A and B), wheat bran (C and D), and corn cob (E and F). A, C and E: Separate hydrolysis: 50 U cellulase (circle) or 50 U xylanase (triangle); simultaneous hydrolysis: 50 U cellulase and 50 U xylanase (inverted triangle); control: no enzyme added (square) to substrates for 16 h; B, D, and F. DS curve of corn stalk (B), wheat bran (D), and corn cob (F).

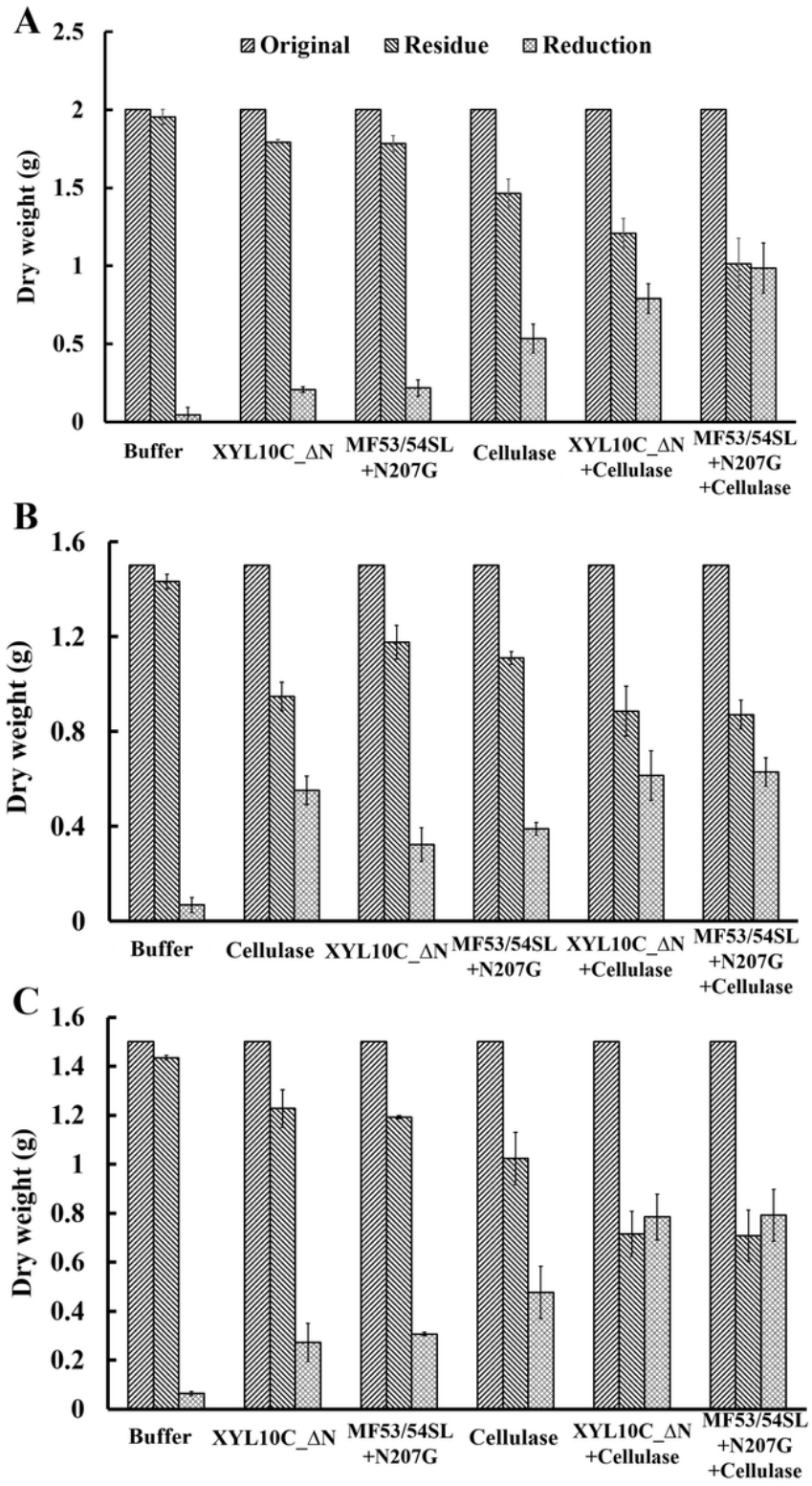

Figure 6

Change in dry weight of biomass during hydrolysis with cellulases and/or xylanase after 24 h. A. corn stalk, B. wheat bran, C. corn cob.

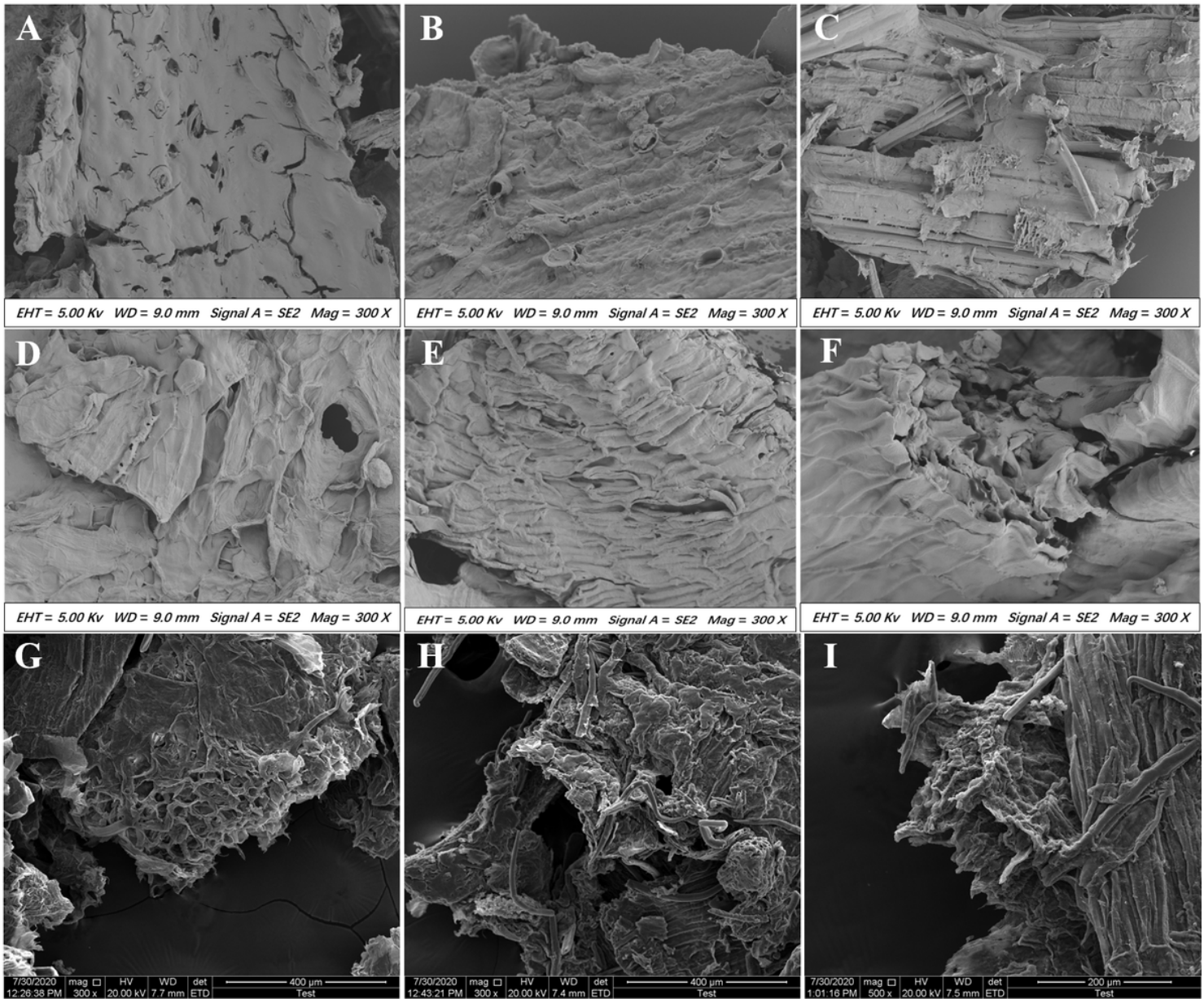

Figure 7

Electron microscopy scan of corn stalk, wheat bran, and corn cob microstructure treated with enzymes. A. Treatment of corn stalk for 24 h by adding MF53/54SL+N207G alone; B. Treatment of corn stalk for 24 h by adding cellulase alone; C. Simultaneous addition of MF53/54SL+N207G and cellulase to treat corn stalk for 24 h. 300 times larger for all images. D, E, F and G, H, I represent the same treatment wheat bran and corn cob, respectively.

Supplementary Files

This is a list of supplementary files associated with this preprint. Click to download.

- GraphicalAbstracts210426.tif

- Supplementmaterial210428.docx